Silver-Decorated TiO_2 for Enhancement of RR4 Dye Degradation Under Photoelectrochemical and Electrochemical Catalyses

Muhammad Afiq Rosli[1], Siti Raihan Hamzah[1], Nureel Imanina Abdul Ghani[1], Nadiah Sabihah Md Natar[1], Nur Aien Muhamad[1], Mohd Azlan Ishak[1], Muhammad Zahiruddin Ramli[2], Mohammad Saifulddin Mohd Azami[1] and Wan Izhan Nawawi[1]*

[1]Faculty of Applied Sciences, Universiti Teknologi MARA, 02600 Arau, Perlis, Malaysia
[2]College of Engineering, Universiti Teknologi MARA Cawangan Pulau Pinang, Kampus Permatang Pauh, 13500 Permatang Pauh, Pulau Pinang
*Corresponding author (e-mail: wi_nawawi@uitm.edu.my)

In this study, a commercially available Degussa P25 TiO_2 was used as a photocatalyst after a modification with silver (Ag) as a dopant to enhance the photocatalytic performance. This is due to the better migration of the generated electrons into the TiO_2 when exposed to light. The preparation of Ag-TiO_2 was conducted via the photo-deposition method, with silver nitrate ($AgNO_3$) mixed with isopropyl alcohol (IPA) and distilled water (DW) as Ag precursor at various ratios of Ag dopant to TiO_2. The immobilization of Ag-TiO_2 was prepared via polymer-based immobilization by using epoxy natural rubber-50 (ENR50) and polyvinyl chloride (PVC) and the obtained photocatalyst was characterized by FESEM-EDS, XRD, 3D Profiler, FTIR and EIS. Photoelectrochemical degradation (PEC) was applied for photocatalytic performance measurement by using reactive red 4 (RR4) dye. The optimum photocatalytic performance of immobilized Ag-TiO_2 was obtained at 24 V, labelled as (APV24), with almost complete degradation of 30 ppm RR4 dye achieved below 10 min under 55 W fluorescent lamp irradiation, which is faster compared to immobilized unmodified TiO_2. The acquired results from FESEM-EDX and XRD analyses indicated the presence of Ag on Ag-TiO_2 with no phase transformation. Based on conductivity study, a significant electron supply was observed on APV24 during the photocatalytic activity tended to generate hydroperoxyl and hydroxyl radicals, contributing to the degradation of the dye and floc formation throughout the process. The APV24 sample had shown the same photocatalytic degradation rate under immobilization due to the polymer-based formulation in the post-preparation of immobilization that was able to retain the photocatalytic activity.

Keywords: Photoelectrochemical; photocatalysis; immobilization titanium dioxide; silver; RR4 dye

Received: December 2023; Accepted: January 2024

Most of the water bodies are currently tainted by various organic dyes. The textile, printing, and dyeing sectors are the primary industries contributing to water contamination. The most common type of dye pollution detected is azo dyes, which seem poisonous and can cause cancer in aquatic life if discharged into the environment [1]. Researchers have observed numerous treatments such as physical, chemical, and biological treatments to reduce organic pollutants [2]. Conventional techniques, such as physical and chemical treatments, are no longer considered ecologically benign due to the production of residue, which requires further treatment and incurs additional costs [3].

The advanced oxidation process (AOP) is one of the desirable methods for removing toxic organic chemicals in wastewater. The hydroxyl group produced by the AOP may oxidize the organic contaminants [4]. Methods such as photocatalysis, photo-Fenton, ozonation, and electrochemical oxidation are examples of AOP. This hydroxyl group is also more potent than any commercialized chemicals, such as aluminium potassium sulfate, used to treat wastewater. Previous researchers have discovered two types of AOP: slurry and immobilized photocatalyst, which have advantages and disadvantages [2]. Even though the slurry AOP has a high photocatalytic activity compared to the immobilized AOP, a further treatment for removing the suspended photocatalyst is required.

Photoelectrochemical (PEC) systems have gained attention for the degradation of high-strength organic pollutants in wastewater. This system lies under electrochemical-AOP, also known as EAOP [5]. PEC recently became attractive because of its effectiveness in producing •OH radicals as compared with the normal photocatalysis process due to additional direct current (DC) applied to the system [6]. Moreover, [7] also states that the PEC system is able to perform a rapid reaction with organic compounds to produce CO_2, water, and inorganic ions.

Besides the degradation of organic pollutants, PEC systems also can be used for water splitting to produce hydrogen (H_2) and oxygen (O_2) gases [8]. H_2 can be used to replace non-renewable energy sources converted into electricity by using green technology [9]. Recently, researchers became interested in studying photoelectrochemical water splitting due to its environment-friendly process as it produces H_2 from solar irradiation to replace non-renewable energy sources [10].

There are several types of photocatalysts that have been studied by past researchers, such as titanium dioxide (TiO_2), zinc oxide (ZnO), zinc sulfide (ZnS), cadmium sulfide (CdS), strontium peroxide (SrO_2), and tungsten trioxide (WO_3). Titanium dioxide (TiO_2) is commonly used by researchers as a photocatalyst in photocatalysis and photoelectrochemical processes due to its high photocatalytic performance, low cost, high stability, and harmlessness compared to other photocatalysts [11]. It is capable of degrading any organic pollutants such as methylene blue (MB) [12], methyl orange (MO) [13], rhodamine blue (RB) [14], and reactive red 4 (RR4) dyes [15]. However, due to its wide bandgap energy, it is limiting the photoactivity performance of TiO_2 in photocatalysis [16]. This limitation can be overcome by modification with metal and non-metal elements.

Metal and non-metal modifications have been extensively explored for the wide optical response of TiO_2. Common noble metals used for the modification on TiO_2 are platinum (Pt) and aurum (Au), but silver (Ag) doping has gained popularity due to its outstanding surface plasmon resonance (SPR) performances [17]. Thus, the photocatalytic activity on degrading organic pollutants during the photocatalysis process can be enhanced and electron-hole pair recombination will be reduced. The presence of Ag doping on TiO_2 in the PEC system makes the produced electrons in the TiO_2 conduction band extremely high for the hydroxyl radicals and superoxide ions production.

EXPERIMENTAL

Chemicals and Materials

Titanium dioxide P25-Degussa was acquired from Evonic-Aeroxide (Germany), epoxidized natural rubber (ENR-50) and polyvinyl chloride (PVC) were supplied by Kumpulan Guthrie Sdn Bhd. (Malaysia) and Merck Sdn. Bhd. (Germany), polyvinyl pyrolidine was provided by R&M chemicals (Malaysia), and ethanol from Hmbg Sdn. Bhd (Malaysia). Reactive red 4 dye (chemical formula: $C_{32}H_{19}ClN_8Na_4O_{14}S_4$, MW: 995.23 g mol^{-1}, λ max: 517 nm) was obtained from Sigma-Aldrich (Germany).

Preparation of Immobilized Ag/TiO_2/ENR/PVC and Ag/TiO_2/PVP/Ethanol

Silver nitrate was used as the Ag precursor, mixed with isopropyl alcohol along with distilled water. The mixture then underwent photodeposition for one (1) hour to make silver well distributed with TiO_2. The prepared sample was then immobilized using two different polymers, (ENR/PVC) and (PVP/Ethanol), and then bound into a conductive substrate. An aluminium plate was used as the solid substrate for TiO_2 to be immobilized for this experiment. The aluminium plate was weighed before the dip-coating process. The clean aluminium plate was dipped into the prepared solution until the solution covered up to 50% of the surfaces and dried by using a hot blower. This dipping process was repeated 2 times and 1 side of the coated plate was removed.

Photocatalytic Measurement

The photocatalytic performance of immobilized Ag-TiO_2/ENR/PVC and Ag-TiO_2/PVP/ethanol was carried out by immersing the aluminium plate into a glass cell that contained 8 ml of 30 ppm RR4 dye (anionic dye) solution. The glass cell was set up with 55 W fluorescent lamp irradiation as the light source, without aeration, and bias applied at 20 to 24 V by using a direct current controllable power supply. The photoelectrochemical performance of immobilized Ag-TiO_2/ENR/PVC was measured by absorbance value detected by monitoring the color degrading of RR4 dye at every 1-minute interval until the dye solution turned colorless. A UV spectrophotometer (DR1900) at 517 nm of wavelength detection was used for the absorbance detection value for RR4.

Characterization Techniques

The surface morphology of the samples was analyzed by using a Scanning Electron Microscope (SEM) analyzer model LEO SUPRA 50 VP Field Emission SEM (Germany) and a 3D Optical Profilometer (PEMTRON HAWK 3D WT-250, Korea). X-ray diffraction (XRD) analysis using Bruker D8 Advance diffractometer was conducted to see the crystallinity of the samples and analyzed against the standard JCPDS library. High-resolution transmission electron microscopy (HRTEM) was used for analyzing the crystallographic structure in differentiating the nanoscale fringes for every compound present. All of the changes in the functional groups of the samples were analyzed with an average of 10 scan from spectrum 4000 – 600 cm^{-1} using a Fourier Transform Infrared – Attenuated Total reflectance (FTIR – ATR) analyzer (Perkin-Elmer, model system 2000 FTIR, USA). Electron impedance spectroscopy was applied in determining the conductivity of the samples in studying the

effectiveness of sample in PEC processes by using the Autolab analyzer from METROHM. Both analyses were done at UiTM Perlis.

RESULTS AND DISCUSSION

In this study, anionic RR4 dye was used as the model pollutant in order to determine the adsorption study of prepared Ag-TiO_2/ENR/PVC under the photo-electrochemical conditions of 55 W of light irradiation, 20/24V electrical bias, and without any aeration. There were 4 different conditions with samples labeled as APV0, AV24, APV20, and APV24. Where, APV24 refers to Ag-TiO_2/ENR/PVC under 24 V applied voltage and 55 W light irradiation (see Table 1). Figure 1 shows the percentage of dye removed during 4 minutes of the photo-electrochemical process (PEC). Based on Figure 1, APV24 removed more than 90% of the dye compared to APV0, which removed only 5% of the dye. This might be due the excessive formation of hydroxyl (OH) and hydroperoxyl ($HO_2\cdot$) radicals which are powerful to degrade the organic pollutant, while reducing the formation of flocs during the PEC process [9]. Table 1 summarizes all the results for the degradation of RR4 dye in 4 minutes with the different conditions on the same setup. From the results that had been obtained, APV24 was chosen as the optimum sample to degrade the RR4 dye due to the high rate constant and percent degradation.

Table 1. Results for degradation of RR4 dye in 4 minutes with different conditions on the same setup.

Sample	Irradiation	Voltage	Rate Constant (min^{-1})	R^2	Percentage removal
APV0	55 W	-	0.0131	0.9966	5.23%
AV24	-	24 V	0.343	0.9592	75.66%
APV20	55 W	20 V	0.6038	0.9336	86.33%
APV24	55 W	24 V	0.6344	0.9819	90.24%

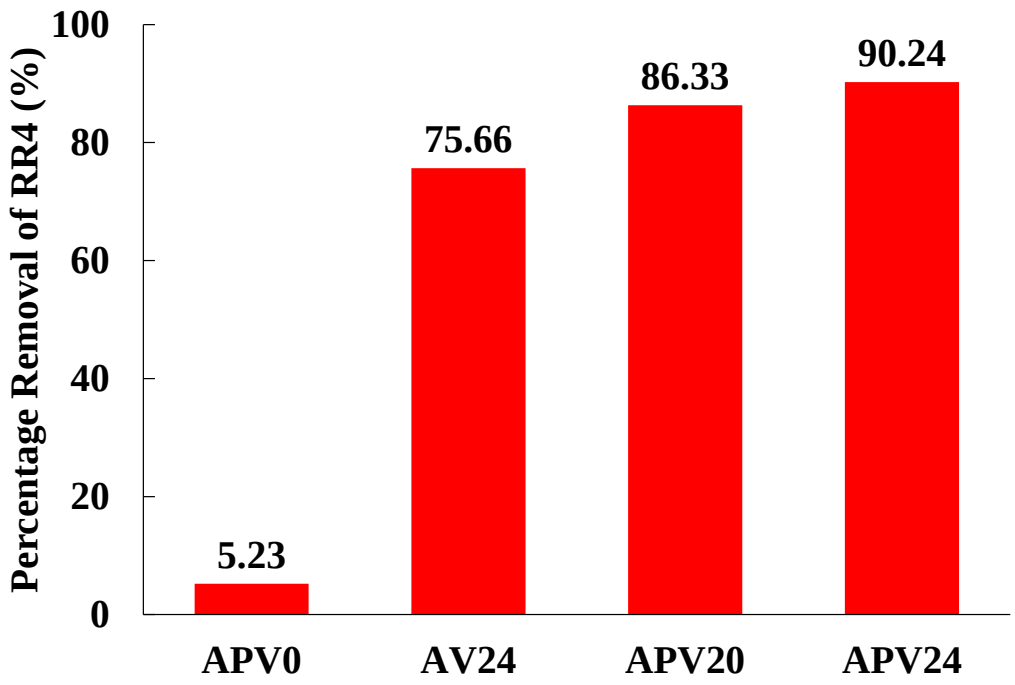

Figure 1. Percentage removal of RR4 dye (%) for each sample respectively after 4 minutes of photoelectrochemical process.

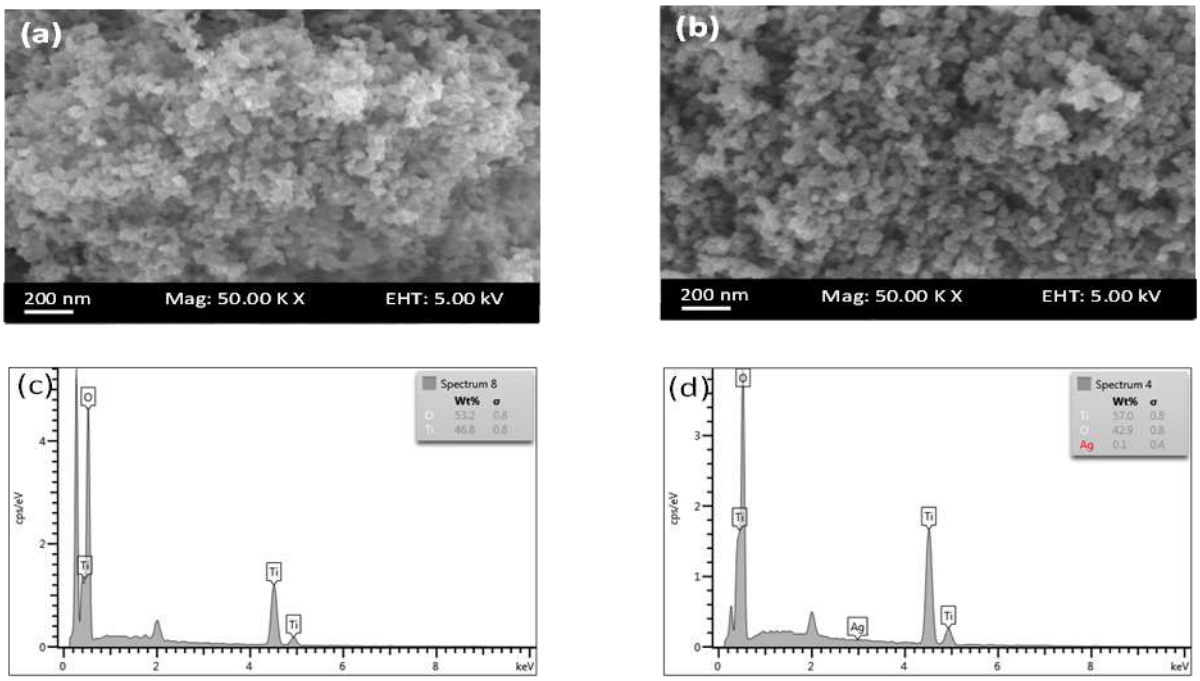

Figure 2. FESEM images of (a) unmodified TiO_2 and (b) APV24 and EDX spectra of (c) unmodified TiO_2 and (d) APV24.

Figure 2 shows the surface morphology via Field Scanning Electron Microscopy (FESEM) at 50.00KX magnification for unmodified TiO_2 and APV24. The TiO_2 particles possessed nearly homogenous spherical shape and size (Figures 2a and b). The EDX analysis was used to confirm the presence of Ag in TiO_2. The weight percentages of Ag, O, and Ti elements in Ag/TiO_2 were found to be 0.1%, 57.0%, and 42.9%, respectively, as shown in Figures 2c and d. The EDX confirmed that silver was present in the TiO_2 particles, where the Ag peak was detected at 3.0 keV. Based on this observation, the presence of silver in the TiO_2 nanocomposite did not destruct the structure of the catalyst after 3% of silver was doped into TiO_2.

The X-Ray Diffraction (XRD) patterns of the unmodified TiO_2 and APV24 samples are presented in Figure 3, where 'A' represents anatase, 'R' for rutile, and 'Ag' for silver. All diffraction peaks for the unmodified TiO_2 and APV24 samples were in line with JCPDS # 00-021-1272 (anatase), JCPDS # 00-021-1276 (rutile), and JCPDS # 00-004-0783 (silver) phases. The diffraction for the APV24 sample of anatase signals was detected at 2θ = 25.67, 38.30, 48.48, 54.43, 62.98, 69.39 and 75.63°, while 27.79, 36.45, 41.80 and 55.45° for rutile. There were 3 peaks detected for Ag peak at 2θ = 38.61°, 64.38° and 83.40°, where these peaks confirmed the presence of silver in the TiO_2. Usually, the XRD peaks will appear for Ag at 38.1 and 64.5° when the Ag doping is more than 2 wt% [18]. The strong diffraction peaks at 25.67° and 48.48° confirmed the samples were in anatase structure. There were no other impurities detected, showing the high purity of the final products. In the XRD analysis, only the crystalline phase of the particles will be detected. The peak intensity of unmodified TiO_2 was low compared to APV24, which was caused by the crystalline phase occurring after the PEC processes. Wang (2014) reported that the photocatalytic performance of anatase nano-particles increases upon an increase in the crystallite size due to the optimization of the optical property and charge carrier dynamics [19]. Table 2 shows all the crystallinity index (CI), crystallite size, *d*-spacing, and specific surface area of the unmodified TiO_2 and APV24 samples.

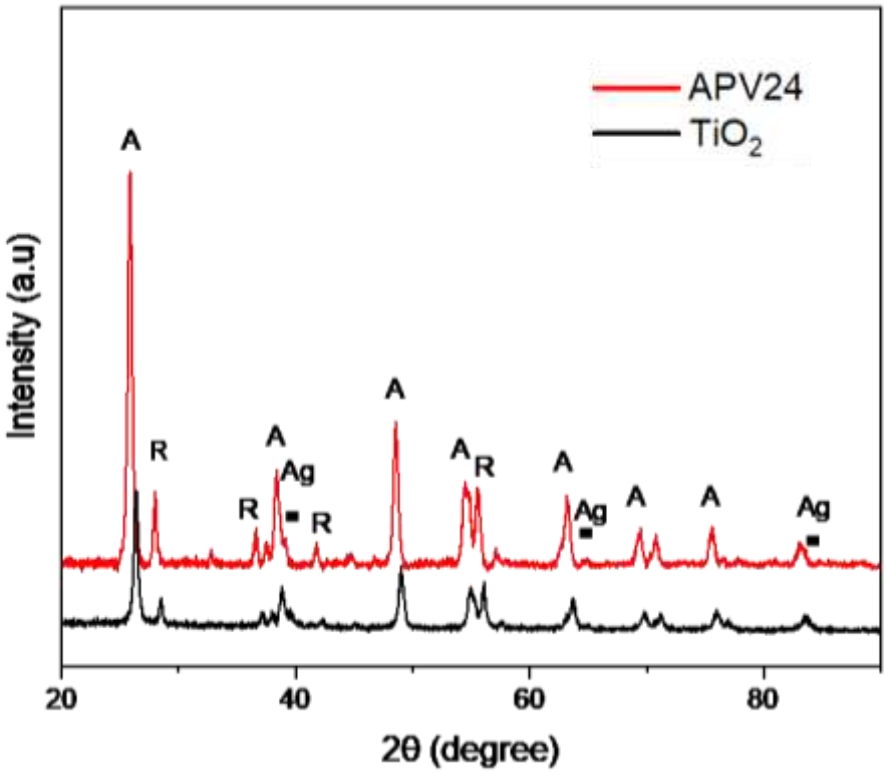

Figure 3. XRD peaks of unmodified TiO_2 and APV24.

Table 2. Crystallinity index (CI), crystallite size, *d*-spacing, and specific surface area of unmodified TiO_2 and APV24.

Sample	Crystallite size (nm)	Crystallinity index (%)	Specific surface area (m^2/g)	*d*-spacing (nm)
TiO_2	6.8203	50.1257	207.9723	2.0463
APV24	6.8862	59.0905	205.9815	1.9838

Surface topography characterization via 3D optical profilometer for APV0 and APV24 is shown in Figures 4a-d. The surface of immobilized Ag-TiO_2/ENR/PVC was changed when undergoing the photoelectrochemical process for a few cycles and the porosity of APV24 was higher compared to APV0. This is due to leaching of the polymer during the PEC process, and this has been proven when the electricity supply would break down the polymer chain [20]. The height of the surface could be determined by the color indicator shown in the 2D surface profiles (Figures 4a and b).

Based on the color indicator, the blue color indicates the deepest height while the red color depicts the tallest height. 3D-surface profile illustrates that the surface of APV24 was more porous compared to APV0, as shown in Figures 4c and d.

The parameters in 2D-surface roughness category are average roughness (R_a) and familiar root-mean-square roughness (R_q). Both parameters are given by the following equations (1-2):

$$R_a = (1/N) \sum_{J=1}^{N} |Z_J| \quad (1)$$

Where N is the total number of measured points and Z_J is the vertical height deviation from the average height of the surface.

$$R_q = \sqrt{(\sum (Z_J)^2) / N} \quad (2)$$

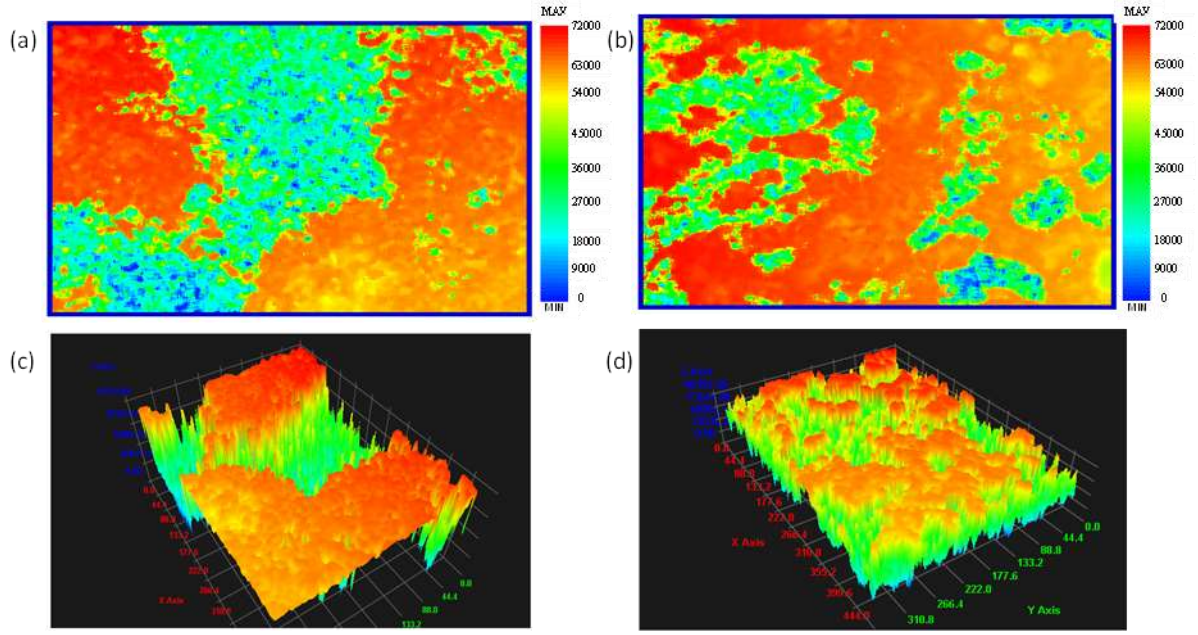

Figure 4. (a) and (b) are 2D results of the height of samples APV0 and APV24 while (c) and (d) are 3D results of the surface of samples APV0 and APV24.

Table 3. Average roughness (R_a), familiar root-mean-square roughness (R_q), minimum and maximum heights of samples APV0 and APV24.

Sample	R_a (nm)	R_q (nm)	Min Height (nm)	Max Height (nm)
APV0	14404.51	16370.84	-15558.97	43950.68
APV24	25216.07	27.121.15	-29326.65	101829.13

In these equations, Z_J is the vertical deviation with respect to a mean line for the *jth* point of the total N measured points. R_a values for APV0 and APV24 were 14404.51 nm and 22201.97 nm, while R_q values were 16370.84 nm and 23032.94 nm, respectively, as shown in Table 3. The surface roughness of APV24 was higher than APV0, which is due to the high porosity as ENR-50 leach out from the immobilized TiO_2 [21].

Figure 5 shows the FTIR spectra of P-25, PVC, ENR TiO_2/ENR/PVC, and APV24 (Ag-TiO_2). Two bands were observed at 3140 and 1625 cm^{-1} that are attributed to O-H stretching and O-H bending vibrations of the hydroxyl group, respectively, and this spectrum has been verified as stated by [22]. The peaks at 1256 cm^{-1} indicate the presence of CH bond in PVC, while the peaks at 1400 cm^{-1} describe the presence of -CH- (asymmetric) in the ENR-50 compound [14]. Moreover, there were peaks detected at 1099 cm^{-1}, which indicate the C-O bond in TiO_2 and has been confirmed in a previous study [23]. However, the peak intensity decreased after the PEC process, as shown in the APV24 spectrum at 1099 cm^{-1} due to leaching out of ENR from the sample [24]. There are several factors affecting the leaching of ENR. First, when electricity is supplied to the immobilized sample, the polymer chain itself would be broken into smaller parts. Second, a few researchers stated that the polymer leach out when in contact with the electrolyte. Based on this observation, it can be concluded that PEC processes were able to reduce the polymer chain due to electrical bias along with the electrolyte.

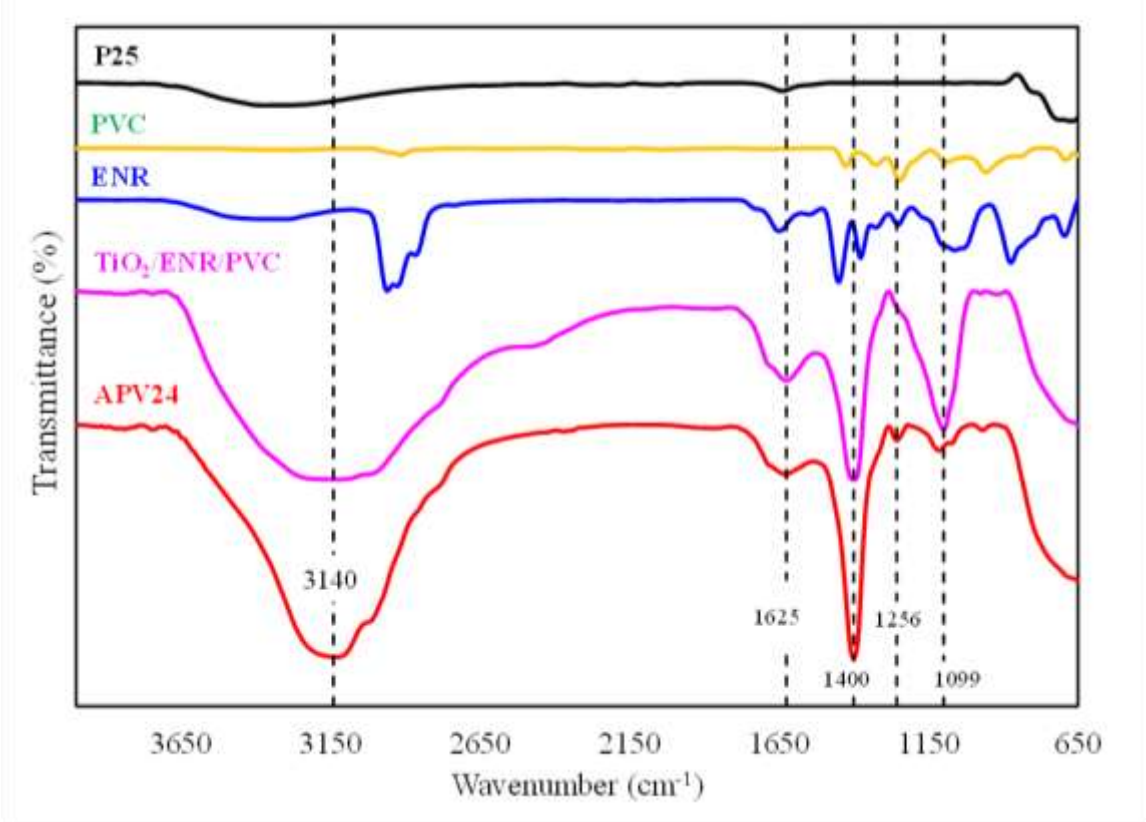

Figure 5. Fourier Transform Infrared (FTIR) spectra (cm^{-1}) of P25, PVC, ENR, TiO_2/PVC/ENR, and APV24.

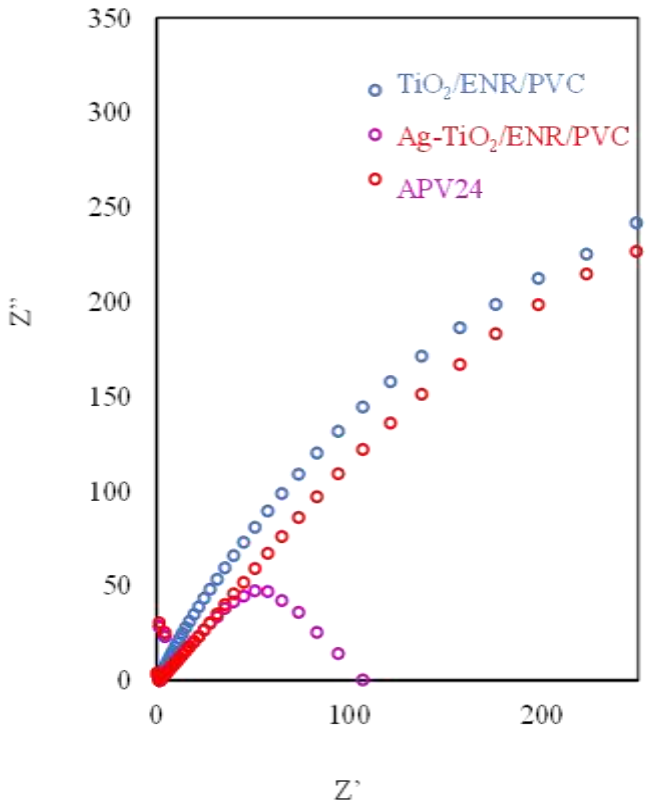

Figure 6. Nyquist plot of TiO_2/ENR/PVC, Ag-TiO_2/ENR/PVC, and APV24 under three electrode reactors (0.5M Na_2SO_4 electrolyte).

To further investigate the contributions of the APV24 electrodes, electrochemical impedance spectroscopy (EIS) plots were measured and compared with TiO_2/ENR/PVC and Ag-TiO_2/ENR/PVC. Figure 6 shows the Nyquist plot of the EIS data obtained which fitted with the RC circuit for the TiO_2/ENR/PVC, Ag-TiO_2/ENR/PVC, and APV24 electrodes. After undergoing the PEC process and doped with Ag, the semicircle radius decreases in the following order: APV24 < Ag-TiO_2/ENR/PVC < TiO_2/ENR/PVC. The charge transfer for bare photoanodes were 49, 329, and 348 Ω. The smaller semicircle radius for the APV24 photoanode indicates an increase in the efficient charge carrier transfer at the electrolyte/electrode interface. Hence, the EIS investigation indicates that the electrolyte ions can be diminished due to the lower charge transfer resistance, which is one of the reasons for the improvement in photocatalytic activity due to effective charge separation and transport.

A graph was plotted for percentage concentration of model pollutant versus irradiation time to determine the rate constant (k) of the degradation of the dye. Langmuir-Hinshelwood pseudo-first order kinetic model states that determination of k will be calculated using formulae (3-4):

$$r = \frac{dc}{dt} = \frac{kKC}{(1+KC)} \quad (3)$$

$$r = kKC = kC \quad (4)$$

Where r is the rate constant, C is the substrate concentration (ppm) at a given time, K is the Langmuir-Hinshelwood adsorption equilibrium constant (ppm^{-1}), and k is the surface reaction rate constant (ppm min^{-1}). KC is negligible concerning time for highly diluted solution ($M<10^{-3}$, $C<108$ ppm). Langmuir-Hinshelwood pseudo-first order kinetic model can also be simplified by using formula (5):

$$\text{In } C_0/C = kt \quad (5)$$

Where:

k = first order rate constant of the reaction (min^{-1})

C_0 = initial concentration of the dye (ppm)

C = concentration of the dye at the respective time (ppm)

and t = irradiation time for the solution.

K will be determined by plotting the graph of percentage of concentration (ln C_0/C) versus irradiation time (t, min). By applying irradiation and voltage in the PEC system, the photocatalytic activity, k values were higher as compared without the presence of irradiation and voltage. Figures 7 a and b show the pseudo-first order rate constant and ln C_0/C values of modified samples. All samples followed pseudo rate constant with R^2 higher than 0.9 (see Figure 7b). APV24 had the highest rate constant (k) value compared to the others, as depicted in Figure 7a. This is due to the reduction of electron-hole recombination from the modifying of silver into TiO_2 and electrolysis in the photoelectrochemical process [25].

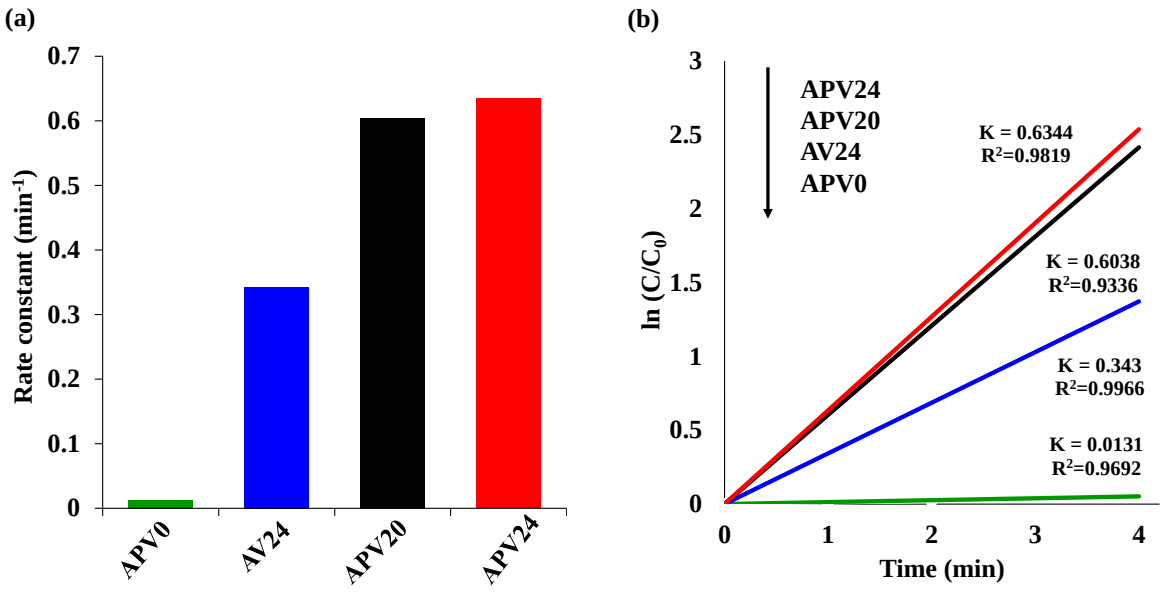

Figure 7. (a) Pseudo-first order rate constant (min^{-1}) and (b) ln C_0/C values for removal of 30 mg L^{-1} RR4 dye via photoelectrochemical process using different samples respectively at 4 minutes.

Table 4. Summary of Ag/TiO_2 nanoparticles for photocatalytic degradation of pollutants.

Reference	Photocatalyst	Pollutant	Efficiency* (times)
This research	TiO_2 (Silver-doped)	Reactive Red 4 (RR4) dye	4.6
Reddy et al. (2023)	Ag-TiO_2	Orange II sodium salt (Azo dye)	0.27
Hou et al. (2021)	Ag nanoparticle sensitized TiO_2 nanotube arrays (Ag/TiO_2 NTAs)	Methylene Blue (MB) dye	1.66
Zou et al. (2019)	(Ag-Ag_2S) titanium dioxide nanorod (TNR) arrays	Methyl orange (MO) dye	1.85
Saquib et al. (2020)	Modified TiO_2 using silver	Methyl orange (MO) dye	2.09

** Based on comparison by fold with unmodified*

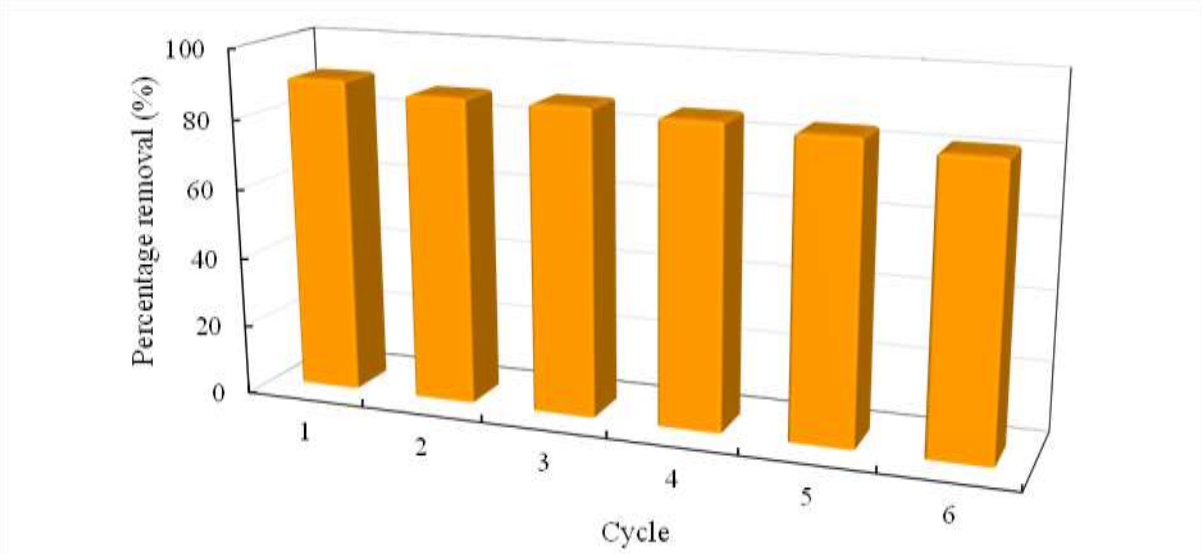

Figure 8. Percentage removal of RR4 dye for APV24 at 5 min in 6 cycles.

As described in Table 4 [26,27,28,29], the photocatalytic efficiencies of our photocatalysts show higher photocatalytic performances as compared to other different groups reported. Several factors, including the quantity of photocatalyst added, dye concentration, light intensity, and the type of pollutant, could contribute to the challenge of comparing the data. The recyclability of APV24 has been analyzed, as illustrated in Figure 8, and the results showed that there was a slight decrement in the percentage removal of the dye due to the reduction of active sites of the photocatalyst. From this observation, APV24 still can be considered as a sustainable sample for the degradation of the RR4 dye.

CONCLUSION

An active photoelectrochemical Ag-TiO_2 has been successfully synthesized via the photo-deposition method with silver nitrate ($AgNO_3$) mixed with isopropyl alcohol (IPA) and distilled water (DW) as Ag precursor. The prepared immobilization of Ag-TiO_2 via polymer-based immobilization by using epoxy natural rubber-50 (ENR50) and polyvinyl chloride (PVC) was characterized by FESEM-EDX, XRD, 3D Profiler, and FTIR. The optimum photocatalytic performance of immobilized Ag-TiO_2 with 24 V, labelled as APV24, almost completely degraded 30 ppm RR4 dye below 10 min under 55 W fluorescent lamp irradiation, which is faster than immobilized unmodified TiO_2. The acquired results from FESEM-EDX and XRD analyses indicated the presence of Ag on Ag-TiO_2 with no phase transformation. Better PEC performance was observed on APV24 due to the high conductivity, high porosity leading to the high decomposition of polymer binder (ENR-50). This research hopefully will help other researchers to produce more facile composites in photoelectrochemical system.

ACKNOWLEDGEMENT

The authors would like to thank Universiti Teknologi MARA (UiTM) for providing the financial support under the internal grant "Dana Pembudayaan Penyelidikan Dalaman" (DPPD), code no: 100-TNCPI/PRI 16/6/2 (012/2023) in conducting this study. We would also like to acknowledge Universiti Malaysia Perlis (UniMAP) and Universiti Teknologi MARA (UiTM) for providing all the facilities.

REFERENCES

1. Cho, H., Joo, H., Kim, H., Kim, J. E., Kang, K. S. & Yoon, J. (2021) Improved photoelectrochemical properties of TiO_2 nanotubes doped with Er and effects on hydrogen production from water splitting. *Chemosphere*, **267**, 129289.

2. Deng, Y. & Zhao, R. (2015) Advanced oxidation processes (AOPs) in wastewater treatment. *Current Pollution Reports*, **1(3)**, 167–176.

3. Ama, O. M. & Arotiba, O. A. (2017) Exfoliated graphite/titanium dioxide for enhanced photo-electronchemical degradation of methylene blue dye under simulated visible light irradiation. *Journal of Electroanalytical Chemistry*, **803**, 157–164.

4. Divyapriya, G., Singh, S., Martínez-Huitle, C. A., Scaria, J., Karim, A. V. & Nidheesh, P. V. (2021) Treatment of real wastewater by photoelectro-chemical methods: An overview. *Chemosphere*, 130188.

5. Khan, M. A., Al-Shankiti, I., Ziani, A., Wehbe, N. & Idriss, H. (2020) A Stable Integrated Photoelectrochemical Reactor for H_2 Production from Water Attains a Solar-to-Hydrogen Efficiency of 18% at 15 Suns and 13% at 207 Suns. *Angewandte Chemie*, **132(35)**, 14912–14918.

6. Garcia-Segura, S. & Brillas, E. (2017) Applied photoelectrocatalysis on the degradation of organic pollutants in wastewaters. *Journal of Photochemistry and Photobiology C: Photo-chemistry Reviews*, **31**, 1–35.

7. Kim, R. N., Yun, H. W., Lee, J., Ryu, S. O. & Kim, W. B. (2021) Enhanced photoelectrochemical performance of Si/TiO_2 with a high atomic density SiO_2 buffer layer. *Applied Surface Science*, **556**, 149712.

8. Natar, N. S., Ikhwan, S., Nazeri, N. S., Hamzah, S. R., Rosli, M. A., Ghani, N. I. & Nawawi, W. I. (2022) Preparation of water-base immobilized N doped TiO2 using DSAT technique for photo-catalytic degradation of methylene blue dye. *Materials Today: Proceedings*, **66**, 4036–4044.

9. Ortiz, A. L., Zaragoza, M. M., Gutiérrez, J. S., da Silva Paula, M. M. & Collins-Martínez, V. (2015) Silver oxidation state effect on the photocatalytic properties of Ag doped TiO_2 for hydrogen production under visible light. *International Journal of Hydrogen Energy*, **40(48)**, 17308–17315.

10. Burton, N. A., Padilla, R. V., Rose, A. & Habibullah, H. (2021) Increasing the efficiency of hydrogen production from solar powered water electrolysis. *Renewable and Sustainable Energy Reviews*, **135**, 110255.

11. Ma, C., Wang, X., Luo, H. & Zhang, D. (2017) Synthesis of Ag/TiO_2 core–shell nanowires with enhanced stability of photocatalytic activity. *Journal of Materials Science: Materials in Electronics*, **28(14)**, 10715–10719.

12. Mousset, E. & Dionysiou, D. D. (2020) Photo-electrochemical reactors for treatment of water and wastewater: a review. *Environmental Chemistry Letters*, **18(4)**, 1301–1318.

13. Razali, M. H. (2019) Methyl Orange Degradation using TiO_2 Powder and Immobilized TiO_2 Photo-catalysts. *Universiti Malaysia Terengganu Journal of Undergraduate Research*, **1(4)**, 61–66.

14. Davaslıoğlu, İ. Ç., Özdokur, K. V., Koçak, S., Çırak, Ç., Çağlar, B., Çırak, B. B. & Ertaş, F. N. (2021) WO_3 decorated TiO_2 nanotube array electrode: Preparation, characterization and superior photoelectrochemical performance for rhodamine B dye degradation. *Journal of Molecular Structure*, **1241**, 130673.

15. Azami, M. S., Ismail, K., Ishak, M. A. M., Zuliahani, A., Hamzah, S. R. & Nawawi, W. I. (2020) Formation of an amorphous carbon nitride/titania composite for photocatalytic degradation of RR4 dye. *Journal of Water Process Engineering*, **35**, 101209.

16. Fonseca-Cervantes, O. R., Pérez-Larios, A., Romero Arellano, V. H., Sulbaran-Rangel, B. & Guzmán González, C. A. (2020) Effects in Band Gap for Photocatalysis in TiO_2 Support by Adding Gold and Ruthenium. *Processes*, **8(9)**, 1032.

17. Ghani, N. I. A., Rosli, M. A., Hamzah, S. R., Natar, N. S., Nazeri, N. S., Ab Aziz, S. I. & Ismail, W. I. N. W. (2022) Water-based Preparation of Immobilized Ag-doped TiO2 Photocatalyst for Photocatalytic Degradation of RR4 Dye. *Science Letters*, **16(2)**, 24–39.

18. Gogoi, D., Namdeo, A., Golder, A. K. & Peela, N. R. (2020) Ag-doped TiO_2 photocatalysts with effective charge transfer for highly efficient

hydrogen production through water splitting. *International Journal of Hydrogen Energy*, **45(4)**, 2729–2744.

19. Wang, X., Sø, L., Su, R., Wendt, S., Hald, P., Mamakhel, A. & Besenbacher, F. (2014) The influence of crystallite size and crystallinity of anatase nanoparticles on the photo-degradation of phenol. *Journal of Catalysis*, **310**, 100–108.

20. Hamzah, S. R., Rosli, M. A., Natar, N. S., Ghani, N. I. A., Muhamad, N. A., Azami, M. S., Ishak, M. A. & Nawawi, W. I. (2023) The Crosslinking and Porosity Surface Effects of Photoetching Process on Immobilized Polymer-Based Titanium Dioxide for the Decolorization of Anionic Dye. *Colorants*, **2(1)**, 73–89.

21. Gu, S., Marianov, A. N., Zhu, Y. & Jiang, Y. (2021) Cobalt porphyrin immobilized on the TiO_2 nanotube electrode for CO_2 electroreduction in aqueous solution. *Journal of Energy Chemistry*, **55**, 219–227.

22. Rioja-Cabanillas, A., Valdesueiro, D., Fernández-Ibáñez, P. & Byrne, J. A. (2020) Hydrogen from wastewater by photocatalytic and photoelectrochemical treatment. *Journal of Physics: Energy*, **3(1)**, 012006.

23. Deshmukh, S. D., Pattebahadur, K. L., Mohod, A. G., Patil, S. S. & Khirade, P. W. (2020) Structural and dynamics study of polar liquid mixtures by dielectric and FTIR spectroscopic characterizations. *Journal of Molecular Liquids*, **297**, 111819

24. Rosli, M. A., Hamzah, S. R., Muhamad, N. A., Abdul, N. I., Ghani, N. S. M. N., Ab Aziz, S. I., Azami, M. S., Ishak, M. A. M., Ramli, M. Z. & Nawawi, W. I. (2022) Acid Photo Etching Effect of Epoxidized Natural Rubber (ENR) and Polyvinyl Chloride (PVC) as Polymer Binder. *Malays. J. Chem.*, **24**, 228–239.

25. Liu, Z., Xu, K., Yu, H. & Sun, Z. (2021) Synergistic effect of Ag/MoS2/TiO2 heterostructure arrays on enhancement of photoelectrochemical and photocatalytic performance. *International Journal of Energy Research*, **45(5)**, 6850–6862.

26. Reddy, N. R., Reddy, P. M., Jyothi, N., Kumar, A. S., Jung, J. H. & Joo, S. W. (2023) Versatile TiO2 bandgap modification with metal, non-metal, noble metal, carbon material, and semiconductor for the photoelectrochemical water splitting and photocatalytic dye degradation performance. *Journal of Alloys and Compounds*, **935**, 167713.

27. Hou, J., Ning, Y., Lu, Y., Zhi, K., Liu, Y., Chen, M. & Wang, Q. (2021) A solar-driven photoelectrochemical platform based on Ag-sensitized TiO2 NTAs for pollutant treatment and hydrogen generation. *Ceramics International*, **47(19)**, 27759–27769.

28. Zuo, Y., Chen, J., Yang, H., Zhang, M., Wang, Y., He, G. & Sun, Z. (2019) Ag-Ag2S quantum-dots modified TiO2 nanorod arrays with enhanced photoelectrochemical and photocatalytic properties. *Journal of Alloys and Compounds*, **780**, 347–354.

29. Saquib, M., Kaushik, R. & Halder, A. (2020) Photoelectrochemical Activity of Ag Coated 2D-TiO2/RGO Heterojunction for Hydrogen Evolution Reaction and Environmental Remediation. *Chemistry Select*, **5(21)**, 6376–6388.